EXPERIMENTAL CRYSTALLIZATION OF Fe-RICH BASALT: APPLICATION TO COOLING RATE AND OXYGEN FUGACITY OF NAKHLITE MIL-03346. J.E. Hammer[1] and M.J. Rutherford[2], [1]Dept. Geology and Geophysics, Univ. Hawaii, Honolulu, HI 96822 (jhammer@soest.hawaii.edu), , [2]Dept. Geological Science, Brown University, Providence, RI 02912

Introduction: The SNC meteorites, including the clinopyroxenite-wherlite group of cumulates, Nakhla, Lafayette, and Governador Valadares, have proven integral for estimating the timing of planetary differentiation, constraining mantle compositions, and interpreting surface reflectance spectra[1,2]. The textures and compositions of these igneous rocks also provide clues about the intensive conditions near the planet's surface. A protracted, sub-surface cooling history at oxidizing conditions has been proposed for the formation of the Nakhlites, based on the nature of chemical disequilibrium between phenocryst phases[3] and compositions of coexisting Fe-Ti oxides[4]. The recently discovered groundmass-rich Nakhlite MIL-03346 provides a new opportunity to assess crystallization conditions of the mesostasis.

Cooling rate and oxygen fugacity was varied in a series of experiments on Fe-rich, Al-poor synthetic starting material in order to evaluate kinetic factors governing the liquid lines of descent, modes, compositions, and textures of rapidly-cooled basalt. The similarities between this material and re-homogenized matrix melt composition of MIL-03346 (Table 1) suggest that crystallization conditions in the natural material may be deduced by comparison.

Table 1.	Na_2O	MgO	Al_2O_3	SiO_2	P_2O_5	K_2O	CaO	TiO_2	FeO	TOT.
This Study[a]	2.13	7.27	9.13	51.4	0.49	0.75	8.77	1.63	18.9	100.4
MIL-03346 GM[a]	2.50	3.40	9.30	49.6	0.65	0.80	9.5	1.70	22.6	100.1

[a]experimental starting material. [b]fused groundmass from Rutherford et al., this volume.

Experimental and Analytical Methods: Fe-rich basalt synthesized from reagents was imparted with an intrinsic fO_2 equivalent to the desired oxygen buffer assemblage, then placed in Mo foil, Pt-Fe alloy, or pure Pt capsules and sealed inside evacuated SiO_2 glass tubes with separate, crimped containers of Fe^o+FeO (IW), SiO_2+Fe_2SiO_4+Fe_3O_4, (QFM), Ni^o+NiO (NNO), or MnO+Mn_3O_4 (MNO). Samples were heated to 1210 °C, annealed for 5 h, and then cooled to <350 °C at one of several constant rates (231, 71, 9, 6, or 3 °C/h).

Quantization of the microtextures included assessment of the volume fraction, ϕ, and the surface area of a crystal population per unit volume of that population, S_V^P [mm^{-1}], which is obtained from BSE images using the mean number of boundary intersections per unit length of randomly-oriented test line, N_L[5]. N_L is obtained by overlaying nested circular test lines, then marking points where the test lines intersect the boundaries between crystals and the surrounding phases. This technique allows parameterization of morphologies that intersect the section plane multiple times and are otherwise difficult to characterize by standard techniques (e.g., CSD analysis). Up to six populations were characterized in each sample: anhedral and euhedral crystals of olivine, pyroxene, and titanomagnetite.

Experimental Results

Phase modes and compositions. Several trends consistently relate mineralogy with the experimental variables. (1) The mode is a strong function of fO_2, with olivine dominating at reducing conditions and titanomagnetite + pyroxene dominating at moderate to high fO_2. There is an apparent proclivity for magnetite and pyroxene crystals to intergrow. (2) Mg contents of pyroxene and titanomagnetite increase systematically with increasing fO_2, while the mean Ti/Al ratio for augite varies inversely with oxygen fugacity (Fig. 1). (3) The range of compositions of phases formed at any given fO_2 and mode is strongly related to cooling rate, where slow cooling produces a more diverse range in composition than rapid cooling. (4) There is no systematic association

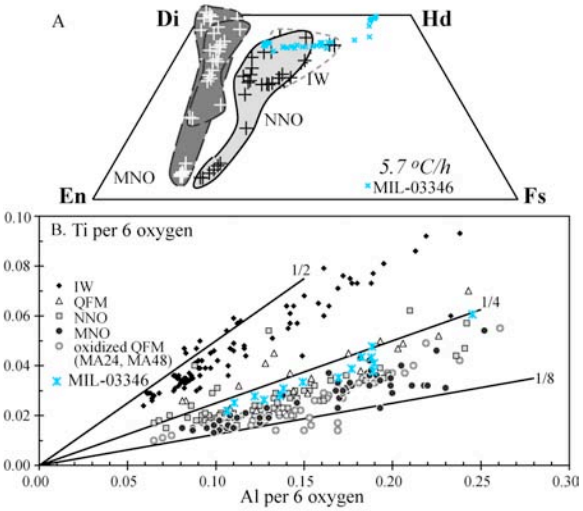

Figure 1. A. Select major element compositions of experimental and natural pyroxenes. MIL-03356 analyses include core-rim traverses of two crystals (Rutherford et al., pers. comm.) B. Minor element ratios in augite vary as a function of oxygen fugacity. MIL-03346 rims extend to higher Al contents (0.46),

between cooling rate and degree of matrix melt differentiation. However, while the volume fraction crystallized at any given cooling rate correlates

inversely with fO_2, the composition of the matrix melts is progressively more evolved as fO_2 increases. For example, matrix melts formed at 72.4 $^oC\ h^{-1}$ are predominantly andesite at IW and predominantly dacite at MNO. (5) At reducing conditions, early crystallization of olivine consumes MgO and drives melts along a Fenner differentiation trend. As fO_2 increases, greater modal Fe-Ti oxide crystallization prohibits Fe enrichment and drives melts along a calc-alkaline trend.

Texture quantization:. Cooling rate exerts the primary control on the size and morphology of the principal phases. Two populations of the principal phases in slower-cooled runs include euhedral (1st generation) and anhedral (2nd generation) morphologies (Fig. 2A). That steady cooling can

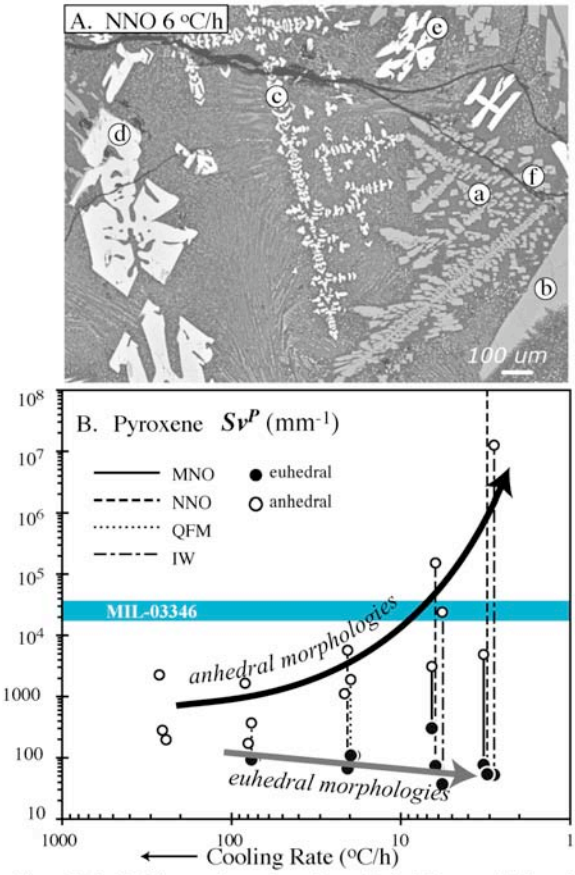

Figure 2. A. BSE image of experimental run. (a) dendritic cpx, (b) faceted cpx, (c) skeletal Fe-rich olivine, (d) hoppered olivine, (e) cruciform titanomagnetite, (f) glass. B. The surface area to volume ratio of anhedral pyroxene (e.g., (a), above) increases as cooling rate decreases, diverging

cause multiple episodes of nucleation (i.e., an unsteady response in the system) is a well-established phenomenon[6] that arises because nucleation requires excess chemical potential driving force to overcome the energy expenditure of forming a solid-melt interface. The existence of two populations of crystals and thus the overall texture are determined by the timing of the second nucleation event with respect to absolute temperature and remaining crystallization time, both of which depend upon degree of initial undercooling.

As expected, populations of anhedral crystals of any given phase generally have significantly greater surface area to volume (Sv^P) ratios than euhedral crystals. The Sv^P ratio of anhedral crystals increases dramatically (>3 orders of magnitude) with decreasing cooling rate, while the Sv^P ratio of euhedral crystals decreases slightly with decreasing cooling rate (Fig. 2B). Therefore, the morphologic contrast between first-nucleated and second-nucleated populations actually *increases* as cooling rate decreases.

Implications for MIL-03346: Preliminary assessment of the meteorite groundmass includes observation of (a) ubiquitous barred fayalitic olivine, (b) cruciform to faceted titanomagnetite, (c) feathery clinopyroxene with high Sv^P (~1.5x10^4 mm^{-1}; Fig. 2B) decorated by titanomagnetite-crystals, (d) increasing core-to-rim Fe contents in pyroxene (Fig 1A), (e) pyroxene rims with Ti/Al ~ 1/4 (Fig. 1B), and (f) interstitial dacite glass (65 wt.% SiO_2).

By comparison with experiments, these features suggest crystallization of the intercumulus liquid in response to mean cooling at 3-6 $^oC/h$, near the NNO buffer. Most importantly, crystallization at IW is ruled out by the ubiquity of titanomagnetite, and the presence of significant olivine eliminates the possibility of highly oxidizing conditions. A moderately oxidizing environment, as proposed, is consistent with the fayalite+magnetite groundmass assemblage in MIL-03346 and analysis of other martian basalts[4,7] ([8]notwithsanding). However, the suggested cooling rate is somewhat faster than is likely for a subsurface cumulate pile[3], and we suggest that the history of MIL-03346 includes extrusion and cooling in a thick lava flow.

References: [1] McSween, H. Y. *Meteoritics* **29**, 757-779 (1994). [2] Borg, L. E., Nyquist, L. E., Wiesmann, H. & Reese, Y. *Geochim Cosmochim Acta* **66**, 2037-2053 (2002). [3] Harvey, R. P. & McSween Jr, H. Y. *Geochim Cosmochim Acta* **56**, 1655-1663 (1992). [4] Reid, A. M. & Bunch, T. E. *Meteoritics* **10**, 317-324 (1975). [5] Underwood, E. E. in *Quantitative Microscopy* (eds. DeHoff, R. T. & Rhines, F. N.) 422 (McGraw-Hill, New York, 1968). [6] Lofgren, G. *Am J Sci* **274**, 243-273 (1974). [7] Herd, C. D. K., Borg, L. E., Jones, J. H. & Papike, J. J. *Geochim Cosmochim Acta* **66**, 2025-2036 (2002). [8] Delano, J. W. & Arculus, R. J. in *LPSC XI* 219-221 (Houston, TX, 1980).